International Journal of Scientific Research and Management (IJSRM)
||Volume||12||Issue||12||Pages||567-580||2024||
Website: https://ijsrm.net ISSN (e): 2321-3418
DOI: 10.18535/ijsrm/v12i12.m02

Numerical Simulation of Flow Behavior in an Open Channel Incoperating A Series of Groins

Suman Jyoti[*1], Monir Hossain[1], Sumon Babu[1], Bishnu Prasad Bhandari[1], Md. Ibrahim[1]

[1]Graduate, Department of Civil Engineering, Dhaka University of Engineering & Technology, Gazipur, Bangladesh.

Abstract
Rivers in Nepal, India and Bangladesh exhibit significant instability due to their loose banks, gentle slopes at both the riverbed and water surface, and irregular sedimentation patterns resulting from substantial sediment loads originating upstream. To mitigate the impact of this instability, groins are constructed along the riverbanks to redirect the flow of water away from areas at risk. However, in numerous instances, traditional groins have proven ineffective. It is essential to conduct comprehensive studies on the performance of groins with various configurations to protect riverbanks from erosion, enhance navigation, and promote the biodiversity of aquatic species. The primary aim of this research is to simulate flow in an open channel using a series of groin models through the application of the 2D numerical model, iRIC Nays2DH. This numerical simulation employs the K-ε model for turbulence and the Cubic Interpolation Pseudo-particle (CIP) method for handling advective terms. Simulation of flow fields due to interaction of series of impermeable, permeable and combined groins placed in a straight channel has been made. A given flow condition is applied for all the groins. The simulation results depict that combined groins in series influence favorable flow fields compared to impermeable and fully permeable groins. This causes water zone near bank at the downstream of impermeable part, then slow flow through the permeable part. No strong circulation of flow at groin field and strong current after the groin head is present.

Keywords : Mitigate, Enhance, Erosion, Influence, Environment Right, iRIC Nays2DH

1. Introduction

Recurrent flood phenomena occurred after heavy rainfall, riverbed and bank of the rivers tend to erode due to high velocity. Also, there are some other reasons for bank erosion like very mild slope in riverbed and water surface, loose sedimentary formation in channel boundaries, small depth of flow due to siltation of huge sediment load coming from upstream, and so on. The simulation of water flow in rivers has been the subject of much research in the field of hydraulics and river engineering (Azevedo et al., 2000). In river and coastal engineering, groins are very important structures for river navigation, coastal protection, and beach reclamation (Sarveram et al., 2012). These hydraulic structures have been constructed in riverbank to deflect the flowing water away from vulnerable zone. The main purpose of building up of such obstacles on natural riverbank is to divert the direction of water flow so that bank erosion can be eliminated. Many experimental and numerical research have been done in order to examine flow pattern and scouring around groins (Francis, 1983), (Rajaratnam and Nwachukwu, 1983), (Tang et al., 2007), (Ali et al., n.d.),(Pourshahbaz et al., 2022), (Haque, 2018). In different conditions of groin length, groin installation angle towards the approaching flow, permeable or impermeable states, submerged and non-submerged states and number of groins, and so on (Maleki and Abbasi, 2023), (Alauddin et al., 2017). Due to the variety in the configuration of groins, flow separation and recirculating length would be greatly different, which is a challenge to the applications of numerical models(Quanhong and Pengzhi, 2007). In stabilizing river channels, groins are extensively used. Impermeable groin imposes a huge obstruction to flow and change the flow profile abruptly. Fully permeable groin cannot modify the flow environment rightly, and flow near bank occurs,

which could affect the bank when associated with oblique flow. Combined groins, which have impermeable parts near bank, could improve the flow field to have favorable environment for groin and bank stability.

In this study, open channel flow with three different arrangements of groins in series – impermeable, permeable and combined groins, is simulated with a two-dimensional (2D) numerical model, iRIC Nays2DH. The main objective of the present study is to investigate flow profiles around different types of groins. So that, the effects of groins in an open channel can be evaluated. The specific objectives are as follows:

To simulate the flow through open channel with groins placed in a series.

To determine the flow fields and compare the channel responses due to three different groin structures.

2. Methodology

In this investigation, the iRIC Nays2DH software is utilized to model the flow dynamics of an open channel that incorporates groins. The International River Interface Cooperative (iRIC) serves as a pre- and post-processing tool and framework tailored for the analysis of flow and sediment transport within river systems. Through its Graphical User Interface (GUI), the application enables users to create, execute, and visualize simulation results. The GUI is equipped with features for constructing both structured and unstructured grids, defining topographical characteristics and boundary conditions, as well as establishing grid-dependent parameters such as grain size, vegetation, and obstacles. This can be accomplished by either mapping observed data onto the grid or by designing user-defined polygons with specific attributes related to grid-dependent values. The software amalgamates the capabilities of MD_SWMS, developed by the U.S. Geological Survey (USGS), and iRIC-Nays, which was created by the Foundation of Hokkaido River Disaster Prevention Research Center.

2.1 Basic equation

2.1.1 K-ε model

The eddy viscosity coefficient within the standard k-ε model can be represented by the subsequent equation:

$$v_t = C_\mu \frac{k^2}{\varepsilon}$$

where, C_μ is a model constant. *k* and ϵ are obtained by the following equations:

$$\frac{\partial k}{\partial t} + u\frac{\partial k}{\partial x} + v\frac{\partial k}{\partial y} = \frac{\partial}{\partial x}\left(\frac{v_t}{\sigma_k}\frac{\partial k}{\partial x}\right) + \frac{\partial}{\partial y}\left(\frac{v_t}{\sigma_k}\frac{\partial k}{\partial y}\right) + P_h + P_{kv} - \varepsilon$$

$$\frac{\partial \varepsilon}{\partial t} + u\frac{\partial \varepsilon}{\partial x} + v\frac{\partial \varepsilon}{\partial y} = \frac{\partial}{\partial x}\left(\frac{v_t}{\sigma_\varepsilon}\frac{\partial \varepsilon}{\partial x}\right) + \frac{\partial}{\partial y}\left(\frac{v_t}{\sigma_\varepsilon}\frac{\partial \varepsilon}{\partial y}\right) + C_{1\varepsilon}\frac{\varepsilon}{k}P_h + P_{\varepsilon v} - C_{2\varepsilon}\frac{\varepsilon^2}{k}$$

2.1.2 Equation of Continuity

The equation of continuity is: $\frac{\partial}{\partial t}\left(\frac{\mathrm{h}}{\mathrm{J}}\right) + \frac{\partial}{\partial \xi}\left(\frac{hu^\xi}{\mathrm{J}}\right) + \frac{\partial}{\partial \eta}\left(\frac{hu^\eta}{\mathrm{J}}\right) = 0$

2.1.3 Equation of Motion

The equation of motion is given as:

$$\frac{\partial u^\xi}{\partial t} + u^\xi\frac{\partial u^\xi}{\partial \xi} + u^\eta\frac{\partial u^\xi}{\partial \eta} + \propto_1 u^\xi u^\xi + \propto_2 u^\xi u^\eta + \propto_3 u^\eta u^\eta$$
$$= -g\left[\left(\xi_x^2 + \xi_y^2\right)\frac{\partial \mathrm{H}}{\partial \xi} + \left(\xi_x\eta_x + \xi_y\eta_y\right)\frac{\partial \mathrm{H}}{\partial \eta}\right]$$
$$-\left(C_f + \frac{1}{2}C_D \propto_s h\right)\frac{u^\xi}{hJ}\sqrt{\left(\eta_y u^\xi + \xi_y u^\eta\right)^2 + \left(-\eta_x u^\xi + \xi_x u^\eta\right)^2} + D^\xi$$

$$\frac{\partial u^{\eta}}{\partial t} + u^{\xi}\frac{\partial u^{\eta}}{\partial \xi} + u^{\eta}\frac{\partial u^{\eta}}{\partial \eta} + \propto_4 u^{\xi}u^{\xi} + \propto_5 u^{\xi}u^{\eta} + \propto_6 u^{\eta}u^{\eta}$$
$$= -g\left[\left(\eta_x\xi_x + \eta_y\xi_y\right)\frac{\partial \mathrm{H}}{\partial \xi} + \left(\eta_x^2 + \eta_y^2\right)\frac{\partial \mathrm{H}}{\partial \eta}\right]$$
$$-\left(C_f + \frac{1}{2}C_D \propto_s h\right)\frac{u^{\eta}}{hJ}\sqrt{\left(\eta_y u^{\xi} - \xi_y u^{\eta}\right)^2 + \left(-\eta_x u^{\xi} + \xi_x u^{\eta}\right)^2} + D^{\eta}$$

where,

$$\propto_1 = \xi_x\frac{\partial^2 x}{\partial \xi^2} + \xi_y\frac{\partial^2 y}{\partial \xi^2}, \propto_2 = 2\left(\xi_x\frac{\partial^2 x}{\partial \xi\,\partial \eta} + \xi_y\frac{\partial^2 y}{\partial \xi\,\partial \eta}\right),$$
$$\propto_3 = \xi_x\frac{\partial^2 x}{\partial \eta^2} + \xi_y\frac{\partial^2 y}{\partial \eta^2}, \qquad \propto_4 = \eta_x\frac{\partial^2 x}{\partial \xi^2} + \eta_y\frac{\partial^2 y}{\partial \xi^2},$$
$$\propto_5 = 2\left(\eta_x\frac{\partial^2 x}{\partial \xi\,\partial \eta} + \eta_y\frac{\partial^2 y}{\partial \xi\,\partial \eta}\right), \propto_6 = \eta_x\frac{\partial^2 x}{\partial \eta^2} + \eta_y\frac{\partial^2 y}{\partial \eta^2}$$

$$D^{\xi} = \left(\xi_x\frac{\partial}{\partial \xi} + \eta_x\frac{\partial}{\partial \eta}\right)\left[v_t\left(\xi_x\frac{\partial u^{\xi}}{\partial \xi} + \eta_x\frac{\partial u^{\xi}}{\partial \eta}\right)\right] + \left(\xi_y\frac{\partial}{\partial \xi} + \eta_y\frac{\partial}{\partial \eta}\right)\left[v_t\left(\xi_y\frac{\partial u^{\xi}}{\partial \xi} + \eta_y\frac{\partial u^{\xi}}{\partial \eta}\right)\right]$$

$$D^{\eta} = \left(\xi_x\frac{\partial}{\partial \xi} + \eta_x\frac{\partial}{\partial \eta}\right)\left[v_t\left(\xi_x\frac{\partial u^{\eta}}{\partial \xi} + \eta_x\frac{\partial u^{\eta}}{\partial \eta}\right)\right] + \left(\xi_y\frac{\partial}{\partial \xi} + \eta_y\frac{\partial}{\partial \eta}\right)\left[v_t\left(\xi_y\frac{\partial u^{\eta}}{\partial \xi} + \eta_y\frac{\partial u^{\eta}}{\partial \eta}\right)\right]$$

$$\xi_x = \frac{\partial \xi}{\partial x}, \xi_y = \frac{\partial \xi}{\partial y}, \eta_x = \frac{\partial \eta}{\partial x}, \eta_y = \frac{\partial \eta}{\partial y}$$

$$u^{\xi} = \xi_x u + \xi_x v, u^{\eta} = \eta_x u + \eta_y v$$

$$J = \frac{1}{x_{\xi}\,y_{\eta} - x_{\eta}y_{\xi}}$$

In relation to the diffusion terms D_{ξ} and D_{η} within the motion equation expressed in general coordinates, the expansion of these terms would significantly increase the number of components involved. Therefore, simplifications are made based on the following assumptions:

It is presumed that the second-order derivative of the metric coefficient is locally negligible. Consequently, these terms are regarded as pseudo-orthogonal coordinates in a local context. As a result, the diffusion terms can be approximated in the following manner:

$$D^{\xi} \cong \frac{\partial}{\partial \xi}\left(v_t\eta_r^2\frac{\partial u^{\xi}}{\partial \xi}\right) + \frac{\partial}{\partial \eta}\left(v_t\eta_r^2\frac{\partial u^{\xi}}{\partial \eta}\right)$$

$$D^{\eta} \cong \frac{\partial}{\partial \xi}\left(v_t\xi_r^2\frac{\partial u^{\eta}}{\partial \xi}\right) + \frac{\partial}{\partial \eta}\left(v_t\eta_r^2\frac{\partial u^{\eta}}{\partial \eta}\right)$$

Where, ξr and ηr are parameters each representing the ratio of the local grid size in general coordinates to the full-scale length of the grid. They are defined as follows:

$$\xi_r = \frac{\Delta\xi}{\Delta\xi'}, \eta_r = \frac{\Delta\eta}{\Delta\eta'}$$

2.1.4 Bottom friction calculation method

In Nays2DH, the bottom friction is determined through the application of Manning's roughness parameter. Users could specify this parameter for each computational cell. The riverbed shearing forces, τ_x and τ_y, are represented by the coefficient of riverbed shearing force, Cf, as outlined below:

$$C_f = \frac{gn_m^2}{h^{\frac{1}{3}}}$$

The Manning roughness parameter can be determined from the relative roughness height, k_s, by applying the Manning-Strickler equation as outlined below.

$$n_m = \frac{k_s^{\frac{1}{6}}}{7.66\sqrt{g}}$$

2.2 Operation procedure of software

The subsequent outlines detail the fundamental procedures for utilizing Nays2DH in conjunction with iRIC.

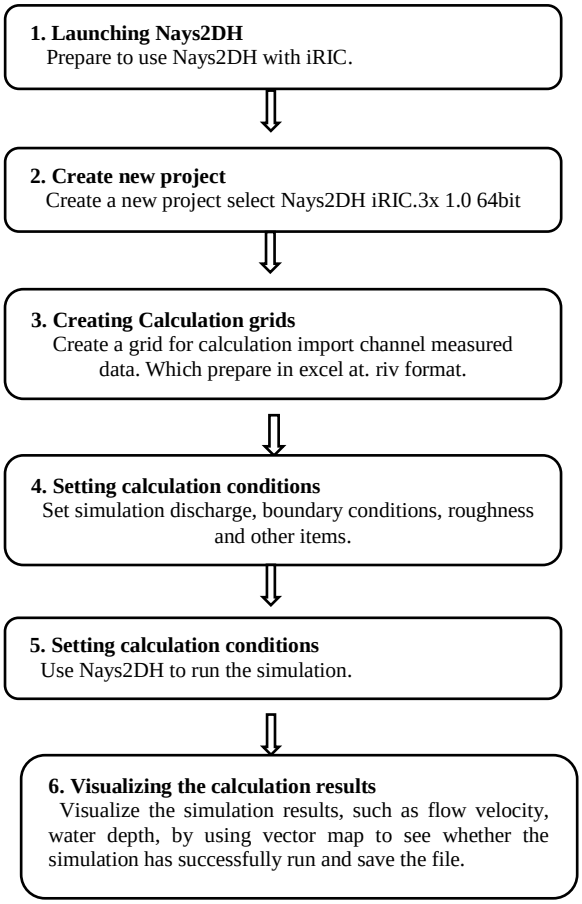

The current study examines three distinct types of groins arranged in series: impermeable, permeable, and a combined variant that incorporates both impermeable and permeable sections. All groins are oriented perpendicular to the channel bank. To predict the turbulent flow field while accounting for anisotropic turbulence, a nonlinear k-ε model is employed. The advection term is addressed using the cubic interpolation pseudo-particle (CIP) method. The fundamental equations are discretized into fully explicit forms and solved sequentially with incremental time steps. An iterative procedure is utilized at each time step to achieve the solution.

The concrete channel under hydraulic engineering laboratory of DUET, Gazipur, which has the dimension of length 20.50 m, width 1.52 m and depth 1.12 m is considered in the numerical simulation. The information of channel and groin models have been presented in Tables 3.2 - 3.5.

2.3 Calculation conditions

A specific flow condition was examined in this study, and it remained consistent across all cases. This condition is detailed below. A constant discharge of 0.05 m^3/sec is used in the simulation. The depth of flow in the channel was kept constant, and it was around 22.5 cm in the channel. The flow discharge remains same for all the cases in this study. Related parameters are given in Table 3.6.

2.4 Working procedure

The numerical simulation works were done as mentioned in the following procedure:

- First, the channel geographic data have been collected and prepared for making calculation grid.
- Then, the geographic data is imported, and grid is created.
- In the grid established in the preceding step, specific locations are designated as obstacle cells to serve as groins, in accordance with the previously outlined groin parameters.
- Subsequently, the conditions for calculation are provided for the computation process. The upstream boundary conditions are defined by a constant discharge, while the downstream boundary conditions are characterized by a constant depth and zero velocity gradients.

The simulations are examined, and the calculation results are extracted for further analyses.

3 Tables

Table: 3. 1 Model Constants

0.09	1.44	1.92	1.0	1.3

The model constants $C1_\varepsilon$, $C2_\varepsilon$, σ_k, and σ_ε are detailed in Table 4.1, with their respective values provided. It is important to note that P_{kv} and $P_{\varepsilon v}$ are determined using the equations outlined below:

$$P_{kv} = C_k \frac{u_*^3}{h} \text{ and } P_{\varepsilon v} = C_\varepsilon \frac{u_*^4}{h^2}$$

Table: 3. 2 Channel dimension

Channel Length	20.50 m
Channel Width	1.52 m
Channel Depth	1.12 m

Table: 3. 3 Groin Parameter (Impermeable)

Length of the groin	0.45m
Thickness of the groin	5cm
Number of groins	5 Nos
Position of first groin	7.5 m from U/S section
c/c distance between groin	0.90m

Table: 3. 4 Groin Parameter (Permeable)

Length of each groin	0.45m
Size of block(each)	3cm
Size of opening(each)	6cm
Thickness of the groin	5cm
Total impermeable portion	15cm
Total permeable portion	30cm
Number of groin	5 Nos
Position of first groin	7.5 m from U/S section
c/c distance between groin	0.90m

Table: 3. 5 Groin Parameter (Combined)

Length of each groin	0.75m
Total impermeable portion	0.45m
First impermeable portion	0.30m
Size of block (each)	3cm
Size of opening (each)	6cm
Thickness of the groin	5cm
Number of groin	5 Nos
Position of first groin	7.5 m from U/S section
c/c distance between groin	0.90m

Table: 3. 6 Flow conditions

Discharge (m^3/sec)	0.05
Depth of flow (m)	0.225
Time period (minutes)	30
Bed slope (So)	0.001

4 Figures And Illustrations

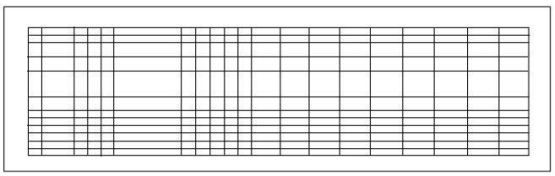

Fig. 4.1 Finite difference grid

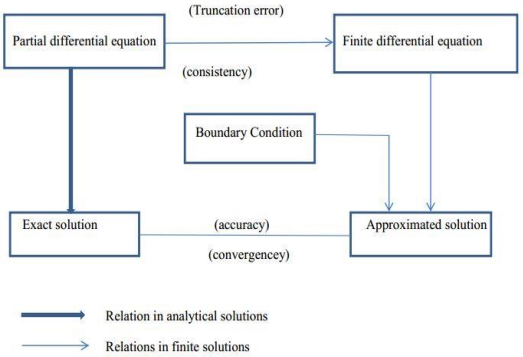

Fig. 4.2 Conceptual relationship between consistency, stability and convergence.

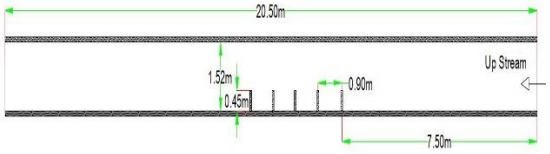

Fig. 4.3 shows model setup

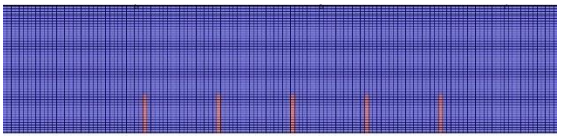

Fig: 4.4 Channel with series of impermeable groin (with grid) on iRIC Nays2DH

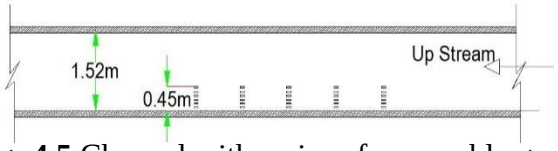

Fig: 4.5 Channel with series of permeable groin

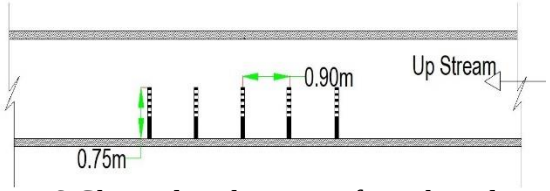

Fig: 4.6 Channel with series of combined groin

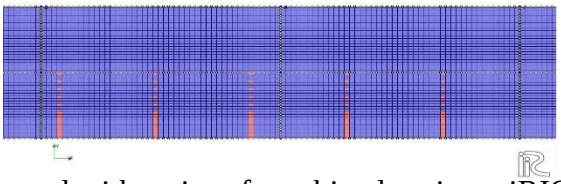

Fig: 4.7 Channel with series of combined groin on iRIC Nays2DH

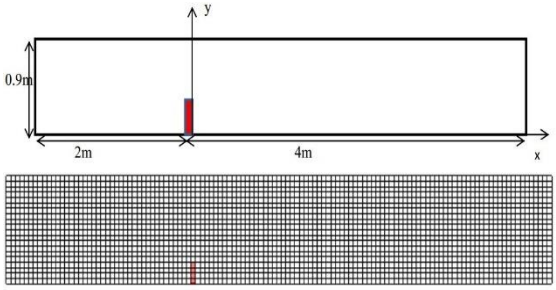

Fig: 4.8 Channel and grids with groin (90° orientation).

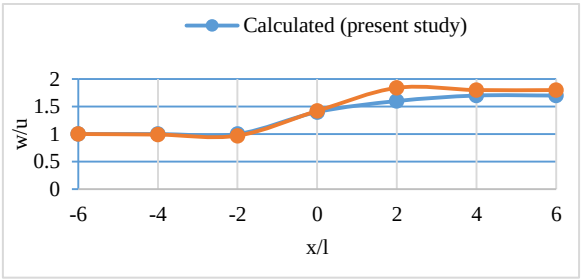

a) Velocity along y/l= 2

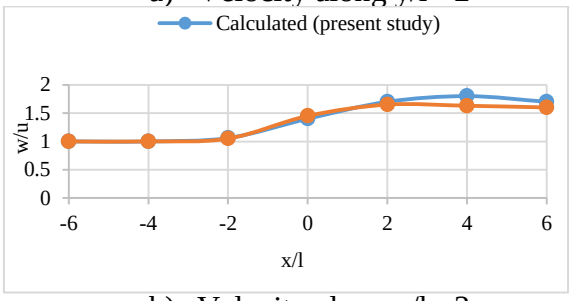

b) Velocity along y/l= 3

Fig: 4.9 Comparison of resultant velocity profile of a) and b) with the available previous study for 90° groin

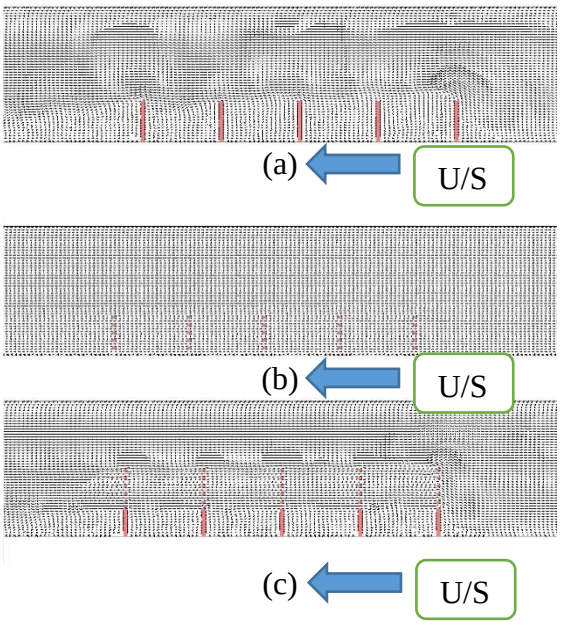

Fig: 4.10 Simulated velocity vectors around the groins for (a) series of impermeable, (b) series of permeable groin, and (c) series of combined groins.

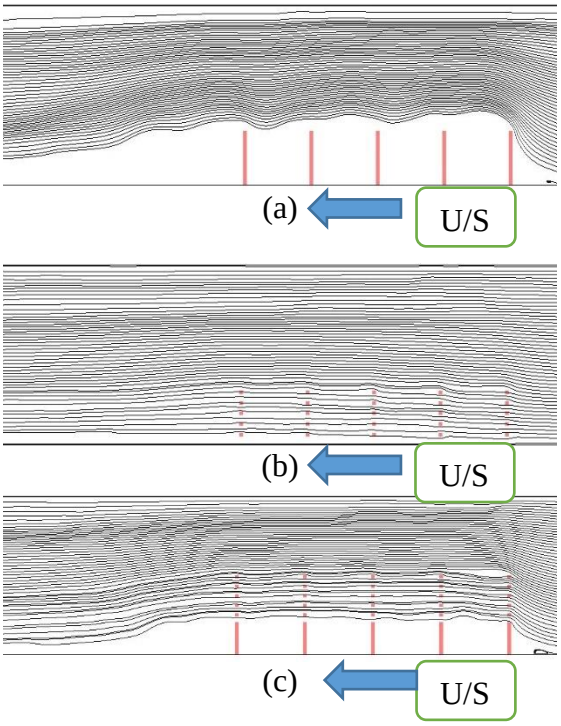

Fig. 4.11 Simulated streamlines around the groins for (a) series of impermeable, (b) series of permeable, and (c) series of combined groins.

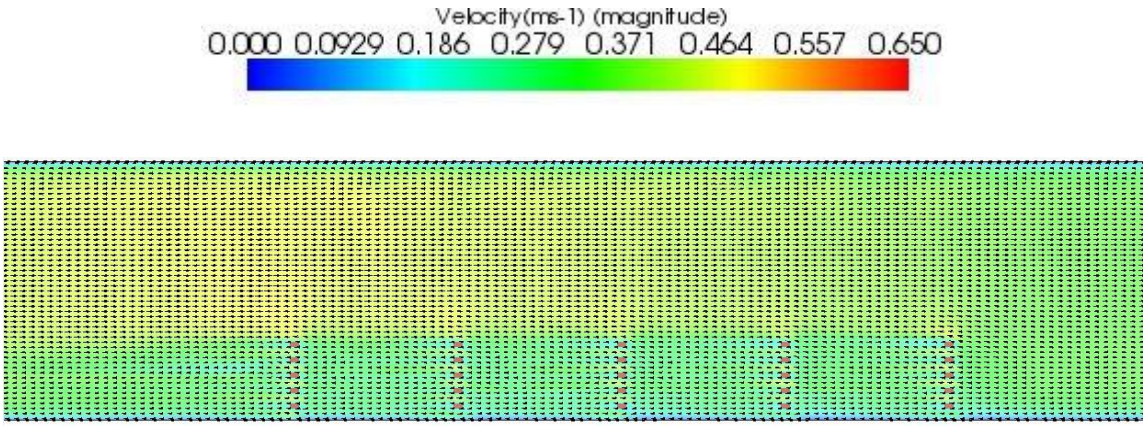

(a)

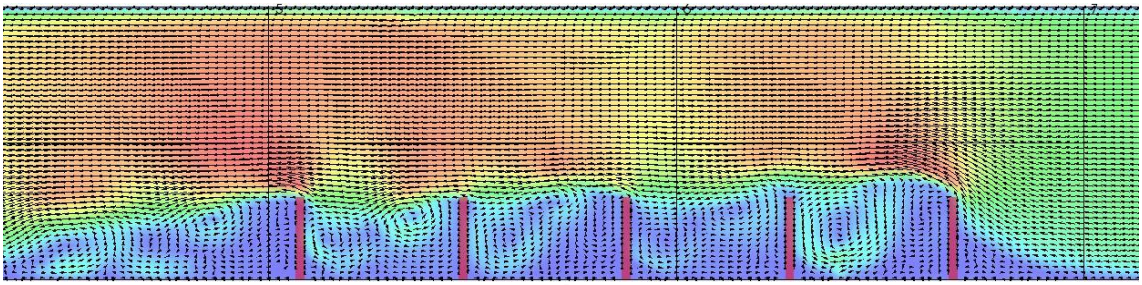

(b)

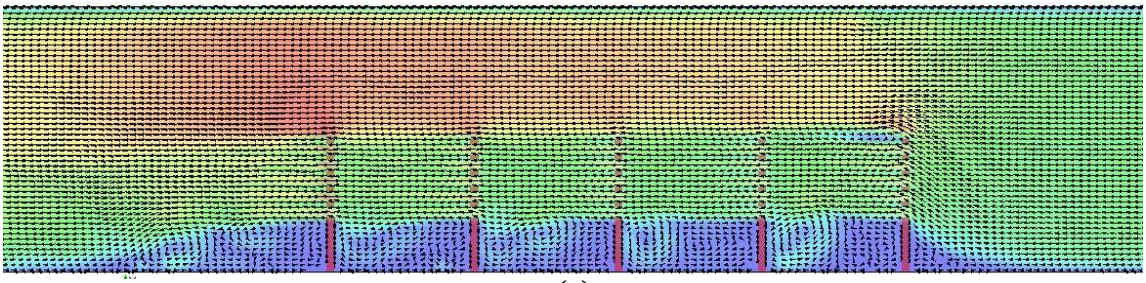

(c)

Fig: 4.12 Velocity magnitude around the groins for (a) series of impermeable (b) series of permeable and (c) series of combined groin.

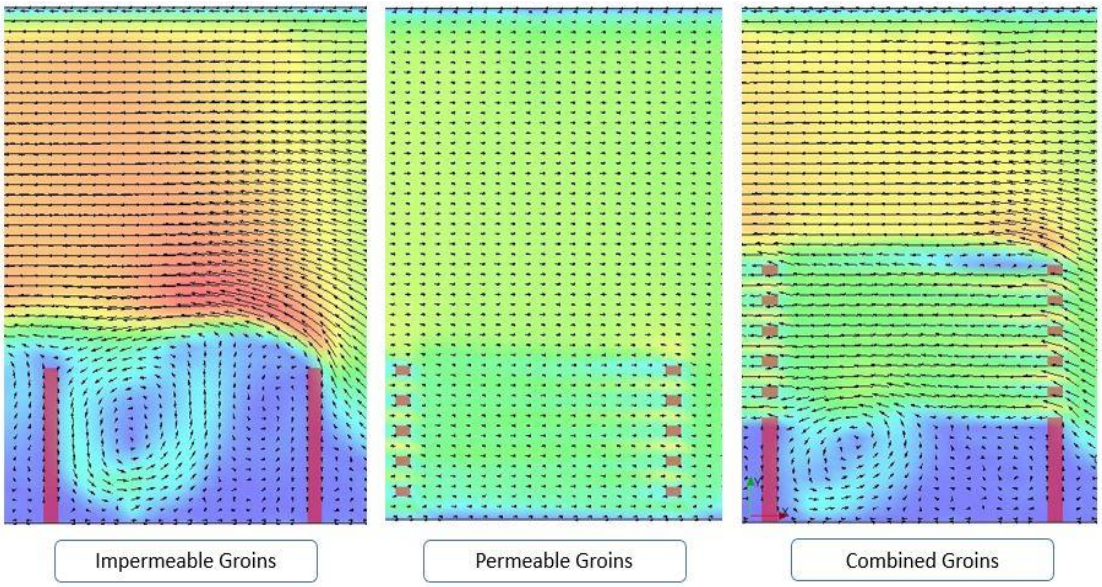

Fig: 4.13 Simulated velocity fields in the 1st groin field.

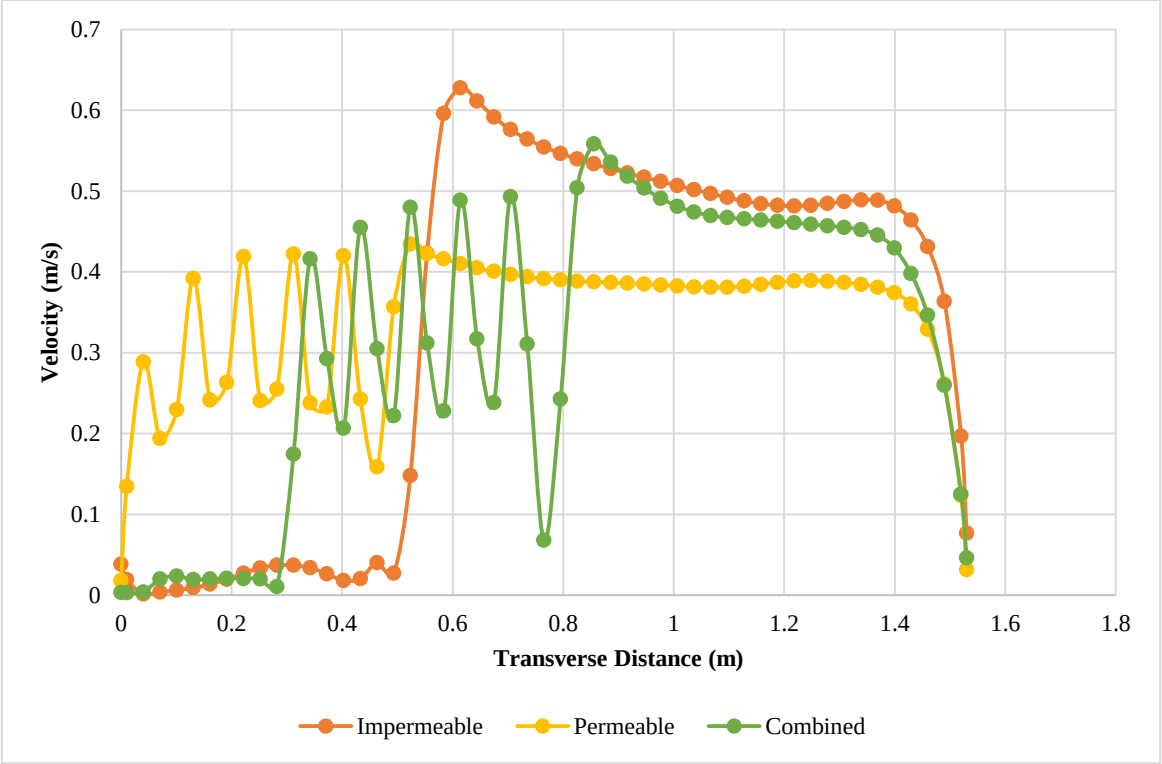

Fig: 4.14 Comparison of simulated velocity profiles along the channel at D/S of 1st groin.

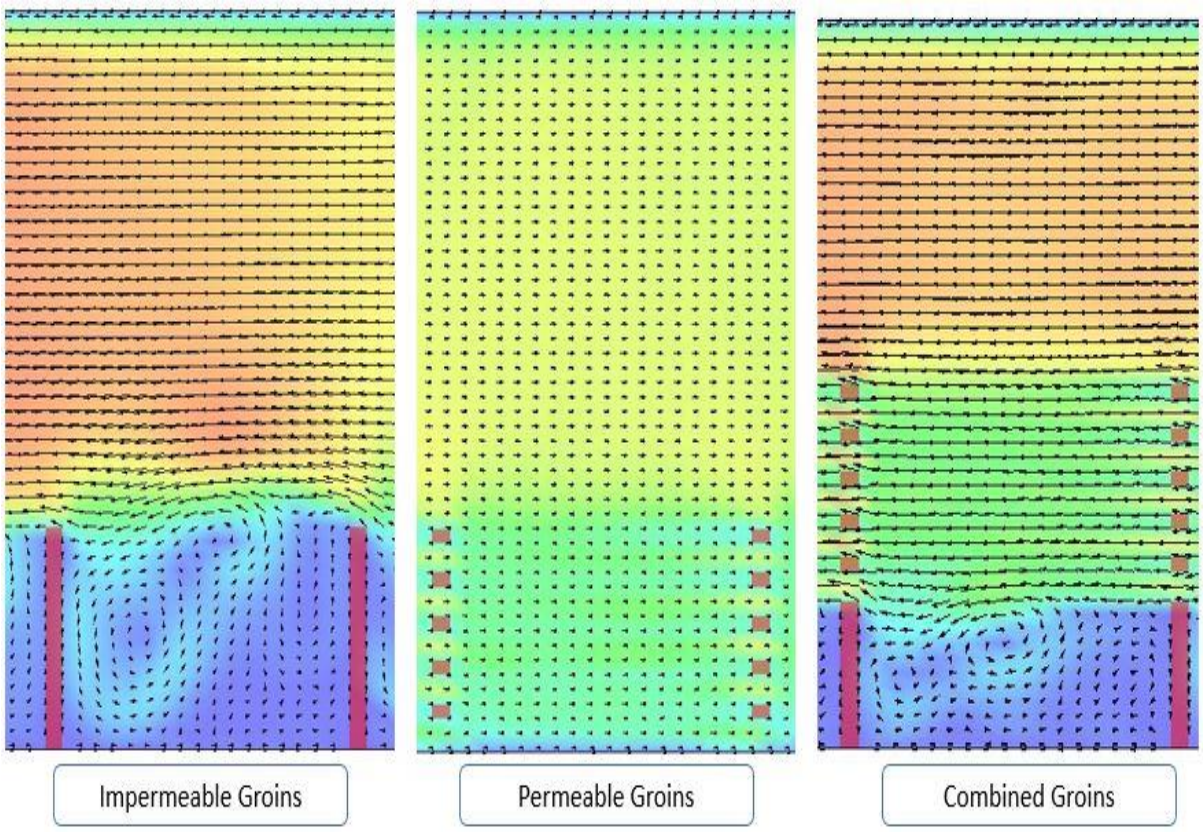

Fig: 4. 15 Simulated velocity fields at the mid portion of 3rd and 4th groin.

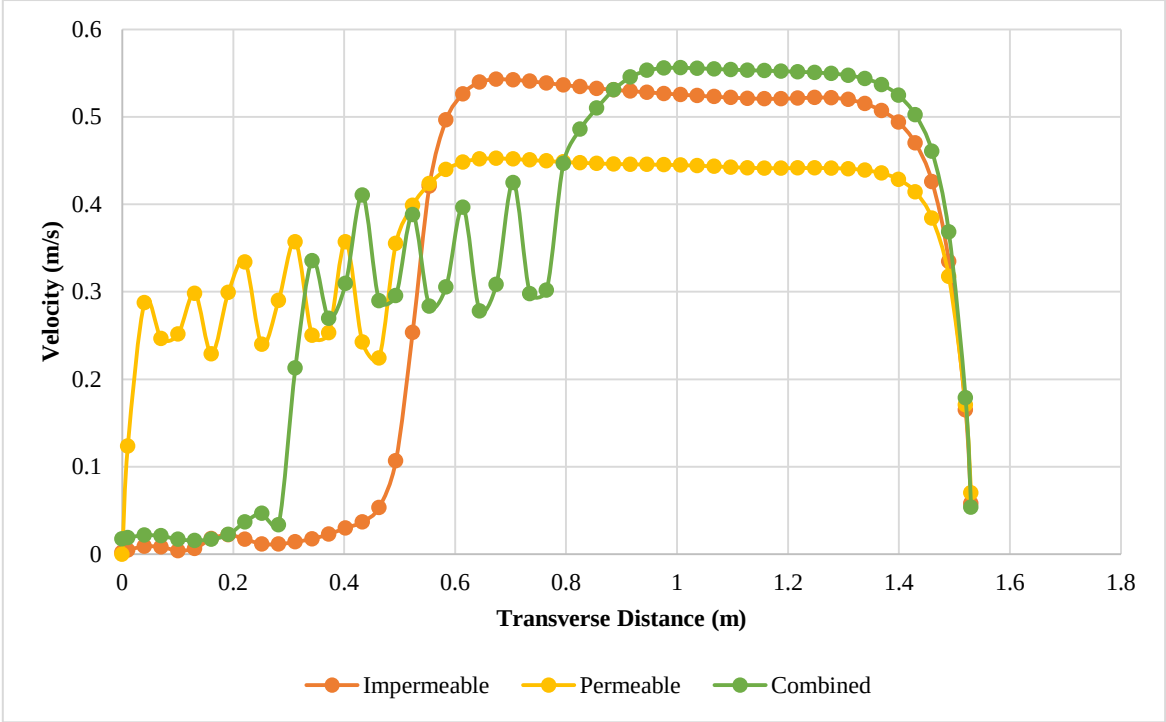

Fig: 4.16 Comparison of simulated velocity profiles at the mid portion between 3rd and 4tn groin.

5 Results And Discussion

5.1 Verification of Numerical Model

The model has been validated against the experimental data provided by (Rajaratnam and Nwachukwu, 1983) who examined the flow fields in a laboratory flume adjacent to a groin-like structure. The numerical model effectively replicates the flow fields of the physical model in areas outside the groin field; however, some inconsistencies are observed downstream of the groin, where the flow exhibits significant skewness. Based on control equations of turbulent flow considering irregular boundary from liquid-solid two phase flow theory, the k - ε model and the Wall Function are adopted to develop a new model (Cui and Zhang, 2006).

A schematic representation of the flow domain for open channel flows with a groin positioned at a 90° angle to the flow direction was created, adhering to the experimental conditions established by (Rajaratnam and Nwachukwu, 1983). The channel dimensions were set at a length of 6 meters, a width of 0.9 meters, a discharge rate of 0.0430 m^3/s, a downstream water depth of 0.001 meters, and a Manning's roughness coefficient of 0.01. For the 90° groins, the resultant velocity profile was compared with the experimental results obtained at y/l = 2 and 3, where l = 141 mm represents the length of the groin. Figure 4.2 illustrates the comparison of the velocity profile for a lateral distance of y/l = 3. The initial flow velocity and water depth were recorded as U_0 = 0.50 m/s and H = 0.189 m, respectively, with velocity normalized by U_0. In the figure, x/l = 0 denotes the position of the groin along the flume.

A distance between enhanced permeable groins equal to four times the effective length of the structure is recommended for a 180° mild flume bend for the investigated particle Froude numbers (Shokrian Hajibehzad et al., 2020). There is a strong correlation between the experimental and calculated results. The velocity profile obtained from iRIC Nays2Dh closely aligns with the experimental data. However, the calculated results tend to underestimate the experimental data in the downstream area of the groin. Similar underestimations were noted in the numerical results provided by (Quanhong and Pengzhi, 2007) and (Sarveram et al., 2012) in this region. This discrepancy may be attributed to the steep velocity gradient present, which renders the depth-averaged model ineffective. the shallow water effect would be lessened after at least some of the proposed excavation plans (Niroshinie et al., 2022). Alternatively, measurement errors in the experimental data could also contribute to these differences. The figure exclusively presents data compared with the experimental findings of Rajaratnam and Nwachukwu illustrated in Figure 4.9.

5.2 Simulated flow fields

Figure 4.10 depicts the simulated velocity vectors of the flow field surrounding the groin for three distinct series of groins under a constant flow condition. The upstream flow in the channel originates from the right side. In all scenarios, the model effectively captures the overall flow characteristics around the groin. The simulation outcomes demonstrate that at the upstream boundary, the flow maintains a uniform state, leading to straight and parallel flow vectors that are aligned with the bank. However, as the flow nears the groin, it is

redirected towards the right bank, unlike the left, due to the obstruction presented by the groin. A recirculation zone is noted immediately downstream of the first groin in the impermeable series.

In the case of permeable groins, the velocity vectors remain undisturbed, similar in length to those in the impermeable scenario. For the impermeable series, the velocity vectors are closely packed in the main channel area following the first groin. In the combined series of groins, the velocity vectors exhibit modifications when compared to both the impermeable and permeable cases, with minor recirculation occurring downstream of each groin along the length.

5.3 Simulated streamlines

Figure 4.11 illustrates the streamlines surrounding a series of groins under various conditions, including impermeable, permeable, and combined series, as derived from the current study. The streamline contour indicates that at the groin head, the flow is redirected towards the opposite bank and downstream of the groin. In the case of permeable groins, the flow traverses through the permeable sections, resulting in less disturbance compared to impermeable groins. The presence of the permeable section in the combined series allows for flow along this area, thereby reducing the velocity intensity at the upper portions of the groins. Figure 4.9 demonstrates that the deviations of streamlines for the series of impermeable groins are greater than those observed in the combined groin series. Conversely, the combined series exhibits the least deviation when compared to the impermeable groin series.

5.4 Comparison of simulated velocity profiles

Fig. 4.12 shows the predicted velocity magnitude of the flow field around the groin for three different series of groins with a constant flow. The results are found to be similar in nature. For all cases, the velocity contour along the left bank is higher than right bank at the downstream region of the groin; it indicates the deflection of flow towards right bank and sheltering of flow by groin at left bank. For the impermeable series of groin, the velocity of flow is very high at just upper position of groins head. The velocity of flow is pick at the first, fourth and fifth groin head.

Though the same length between impermeable and permeable groin the velocity is very low for permeable groins. It is due to in the permeable series of groin the total impermeable length is 15cm, where the impermeable groins total impermeable length is 45cm. At the same time for the combined series of groin the velocity is pick after the groins head, but the intensity of flow velocity is comparatively low than impermeable series of groin. For the combined series of groin, the velocity intensity at the impermeable zone is very low and in the permeable zone flow intensity increase very slowly. Though large dead zone occurs at the downstream of series impermeable groin but here also produced one or more recirculation with high velocity. Scouring have done in this area. So, the stability of groins structure is affected by scouring. In the series combined groin, the velocity intensity very large at the 5^{th} groin head. In the interior of the series combined groin, the dead zone occurs that is comparatively large, and the recirculating area is small with low velocity with respect to impermeable series of groin.

The figure given below (Fig. 4.13) shows the predicted velocity profiles for series of impermeable, permeable and series of combined groin at different points along the channel. For each circumstance, the longitudinal velocity profiles are compared at a lateral position of the channel bed. In the graph, horizontal axis presents the velocity magnitudes of the flow, and the vertical axis represent the lateral distance of the channel bed. Figure 4.13 represents the position of 1^{st} groin D/S and 2^{nd} groin U/S portion in different series groin case. Figure 4.14 represents the flow velocity at the downstream of the 1^{st} groin along the channel width. Each figure shows the comparison the velocity intensity in this area produced by the series of impermeable, permeable and series of combined groin. The velocity intensity produced by the impermeable groin at the D/S along the groin length is very low intensity. The velocity intensity reached at pick position just upper the position of the groin head. For permeable series of groin condition, the velocity along the groin length is high with respect to impermeable series of groins. The velocity intensity through the width of channel is medium due to the resistant portion is very small comparatively impermeable groins. At the same time for the combined groin, the velocity intensity in the impermeable zone is lower than the impermeable groin. After the impermeable zone the velocity intensity rise a small portion and varies depending upon the permeable and impermeable portion along the length of the groin. At the groin head the velocity increase slightly but the intensity is low rather than impermeable groin head. In this point a dead zone produced by impermeable and combined groin but for permeable groin no dead zone produced. Single but large recirculation produced by impermeable groin, for permeable groin no recirculation produced and for combined groin single recirculation produced a low flow intensity.

Fig. 4.15 represents the mid groin field, i.e area bounded by 3^{rd} and 4^{th} groin for all groin cases. Fig. 4.16 represents the flow velocity at the middle of the 3^{rd} and 4^{th} groin along the channel width. The graph shows the evaluation of velocity intensity in middle position along the width produced by the series of impermeable, permeable and series of combined groins. Here the flow velocity intensity for the impermeable groin is very low along the length of groin and after the groin head the velocity is instantly higher. For the permeable groins the velocity has a small change with respect to impermeable groins. At the same time the velocity intensity for the combined groin is comparatively low in the impermeable zone. In

the permeable zone the velocity intensity is increase but lower than velocity intensity produced by impermeable groin. The pick flow occurs after a certain distance from the head of combined groins. This makes the combined groin more stable in sustainable life. In impermeable groin condition approximate two large recirculation produced and for combined groin two small recirculation produced. Due to the high velocity no deposition occurs in that area and maintain the flow depth. Though the total impermeable portion between impermeable and combined groins are same but the velocity reduction pattern is very good for combined groins and the dead zone produced by combined groins is large. The size of recirculation area also small.

From the simulation data, this can be found that installation of permeable groin produces slow flow near side or bank. Although, a dead zone is created in the groin field due to impermeable groin, strong recirculation of flow might be present which can attack the bank line. The flow velocity near the head of the impermeable groin is found very high. So that the possibility of scouring near groin is very high, and thus stability of the groin might be hampered. As the length of permeable groin was kept same of impermeable one, velocity at main channel area is not increased enough, which could assist improving navigation facility. In permeable groin condition though the velocity reduced but no dead zone produced at the groin bank side. In the combined series of groins, the total impermeable portion is same as impermeable groin. Even though, this has same obstruction, because of the presence of permeable part with impermeable part, velocity of flow is not increased much near the head of groin; so that, less scour might be expected. In addition, due to the impermeable portion near bank, a dead zone of less circulation of flow is created which might influence deposition of sediment near bank.

6 Conclusion

This research provides comprehensive insights into the flow fields generated by groins in an open channel. The numerical simulations effectively replicate the overall flow characteristics surrounding a groin. The flow fields identified in this study can be characterized as follows:

- The flow on the upstream side is consistent.
- A circulation of flow is observed downstream of the groin, which is attributed to the flow being sheltered by the impermeable groin.
- High velocity zone is created after the groin due to the deflected flow.

From the comparison of flow profiles due to series of impermeable, permeable and combined groins, this is observed that the velocity is maximum near the head of impermeable groin, and this is much less for permeable and combined groins. Strong circulation of flow is present for impermeable groin; however, a dead zone of less circulation is created near side of channel due to combined groin.

7 Recommendation

Following recommendation can be made for further research:

- The research can be expanded to include simulations of sediment transport, nutrient transport, and bed deformation resulting from the presence of groins.
- Given that the flow dynamics around a groin exhibit significant three-dimensional characteristics, it is advisable to employ a three-dimensional numerical model to investigate flow vortices and localized scour.
- Additionally, the model can be utilized to analyze various spacing configurations between two groins to assess the impact of spacing.
- Furthermore, the study can be broadened to examine different ratios of groin length to channel width, thereby evaluating the influence of groin length on the flow field and sediment transport processes.

References

1 Alauddin, M., Hossain, M., Uddin, M., Haque, M., 2017. A review on hydraulic and morphological characteristics in river channels due to spurs. International Journal of Geological and Environmental Engineering 11, 397–404.

2 Ali, T., Alauddin, M., Alam, J., Hossain, S., Hossain, M., n.d. Effect of Minor Groin on the Downstream Groin Area.
3 Azevedo, L.G.T. de, Gates, T.K., Fontane, D.G., Labadie, J.W., Porto, R.L., 2000. Integration of water quantity and quality in strategic river basin planning. Journal of water resources planning and management 126, 85–97.
4 Cui, Z., Zhang, X., 2006. Flow and sediment simulation around spur dike with free surface using 3-D turbulent model. Journal of Hydrodynamics 18, 232–239.
5 Francis, R.C., 1983. Experiential effects on agonistic behavior in the paradise fish, Macropodus opercularis. Behaviour 292–313.
6 Haque, M., 2018. Simulation of Flow and Sediment Transport in an Open Channel with Obstacle Using IRIC NAYS2DH.
7 Maleki, F., Abbasi, S., 2023. Influence of permeable groins with radial arrangement on local scour around groins: an experimental study. International Journal of River Basin Management 21, 409–420.
8 Niroshinie, M., Ono, N., Shimizu, Y., Egami, K., 2022. Flow Analysis for Navigation Safety by Using iRIC Model Nays2DH, in: Smart Rivers. Springer, pp. 857–867.
9 Pourshahbaz, H., Abbasi, S., Pandey, M., Pu, J.H., Taghvaei, P., Tofangdar, N., 2022. Morphology and hydrodynamics numerical simulation around groynes. ISH Journal of Hydraulic Engineering 28, 53–61.
10 Quanhong, L., Pengzhi, L., 2007. Numerical simulation of recirculating flow near a groyne. Presented at the Proceedings of the The 2nd International Conference on Marine Research and Transportation, pp. 61–68.
11 Rajaratnam, N., Nwachukwu, B.A., 1983. Flow near groin-like structures. Journal of Hydraulic Engineering 109, 463–480.
12 Sarveram, H., Shamsai, A., Banihashemi, M.A., 2012. Two-dimensional simulation of flow pattern around a groyne using semi-implicit semi-Lagrangian method. International Journal of Physical Sciences 7, 2775–2783.
13 Shokrian Hajibehzad, M., Shafai Bejestan, M., Ferro, V., 2020. Investigating the performance of enhanced permeable groins in series. Water 12, 3531.
14 Tang, X., Ding, X., Chen, Z., 2007. Experimental and numerical investigations on secondary flows and sedimentations behind a spur dike. Journal of Hydrodynamics 19, 23–29.